

Adsorption–desorption of Zn^{2+} ions using hydroxyapatite and recovery of zinc by electrochemical precipitation method into deep eutectic solvent

Le Thi Duyen^{a,b,c,*}, Cong Tien Dung^{a,b}, Dinh Thi Mai Thanh^d, Nguyen Thu Phuong^e

^a Department of Chemistry, Faculty of Basic Science, Hanoi University of Mining and Geology, Ha Noi, Viet Nam

^b BSASD Research Group, Faculty of Basic Science, Hanoi University of Mining and Geology, Ha Noi, Viet Nam

^c HiTech-CEAE Research Team, Hanoi University of Mining and Geology, Ha Noi, Viet Nam

^d University of Science and Technology of Hanoi, Vietnam Academy of Science and Technology, 18 Hoang Quoc Viet, Cau Giay District, Ha Noi, Viet Nam

^e Institute for Tropical Technology, Vietnam Academy of Science and Technology, 18 Hoang Quoc Viet, Cau Giay District, Ha Noi, Viet Nam

ARTICLE INFO

Keywords:

Hydroxyapatite

Adsorption

Desorption

Recovery

Zn^{2+} ion

ABSTRACT

Hydroxyapatite has a nanostructure, the chemical formula of $\text{Ca}_{10}(\text{PO}_4)_6(\text{OH})_2$ and a specific surface area of $91.42 \text{ m}^2/\text{g}$. In this paper, hydroxyapatite is used to adsorb Zn^{2+} ions as effective adsorbent. The influence of some factors on Zn^{2+} adsorption capacity and efficiency has been studied. Under the suitable adsorption conditions were hydroxyapatite mass of 0.15 g in 50 mL solution, 50 mg L^{-1} initial Zn^{2+} concentration, pH 5.0, exposure time of 60 min at room temperature (25°C), Zn^{2+} adsorption efficiency and capacity reached 94.79 % and 15.80 mg g^{-1} , respectively. The process of desorption of Zn^{2+} from the loaded adsorbent and recovery of metallic Zn was also investigated. Zinc recovery efficiency reached 93.26 % under appropriate conditions such as applied current intensity of 7.5 mA, electrolysis time of 10 h, loaded hydroxyapatite mass of 0.1 g, temperature 60°C . After desorption process, the adsorbent was regenerated for further studies. The adsorption isotherm was studied based on three Langmuir, Freundlich and Redlich-Peterson models. The adsorption thermodynamics were investigated and calculating the parameters. The adsorption kinetics were examined using two pseudo-first-order and pseudo-second-order kinetic models. The negative value of Gibb's free energy change showed that the adsorption process was feasible and spontaneous in nature. The positive value of enthalpy change indicated that the process was endothermic. The positive value of entropy change showed increased randomness at the solid and solution interface.

1. Introduction

Global development of industrialization is a main factor leading to the water pollution with many chemicals including heavy metal ions leading to the severe health issues. Therefore, there is a deep need to deliver novel water purification methods that could be fast and cost-effective. There are many studies to be proposed in heavy metal ions treatment in water and wastewater such as: chemical precipitation, electrochemical precipitation, membrane separation, ion exchange, adsorption, biological methods, etc., where the adsorption offers versatile application with low costs of the operation. In recent years, adsorbent materials of natural origin such as laterite, basalt, red mud [1], zeolite [2], bentonite [3], kaolinite [4], apatite [5–8], halosite [9–11], natural polymers: chitin, chitosan, starch [12], mesoporous materials prepared from biomass waste [13,14] and agricultural by-

products [15–17], are of great interest to scientists around the world, especially used for wastewater treatment, due to their advantages of, high adsorption efficiency, environmentally friendliness, and the economical aspects. Nevertheless, the effectiveness of the heavy metal ions depends on many conditions as well as the type of heavy metal ions. Zinc is an essential trace element in the body while its excessive exposure can be harmful leading to the diseases such as diabetes, cardiovascular disease, cancer, neurological disorders [18]. Hence, removing zinc from contaminated water sources is very important. Many papers studying on zinc adsorption have been published, in which the adsorbent materials such as thiophene containing mesoporous polymers [19], activated carbon [20], bioadsorbent compounds based agricultural wastes such as orange peel, banana peel, kiwi [21], iron-ore sludge [22] were used. P. Sowmya et al synthesized two novel mesoporous polymers poly [(1E,4E)-1,5-Di-2-thienylpenta-1,4-dien-3-one] (PTCA) and poly

* Corresponding author at: Department of Chemistry, Faculty of Basic Science, Hanoi University of Mining and Geology, Ha Noi, Viet Nam.

E-mail address: lethiduyen@humg.edu.vn (L. Thi Duyen).

<https://doi.org/10.1016/j.poly.2024.117126>

Received 14 March 2024; Accepted 24 June 2024

Available online 29 June 2024

0277-5387/© 2024 Elsevier Ltd. All rights reserved, including those for text and data mining, AI training, and similar technologies.

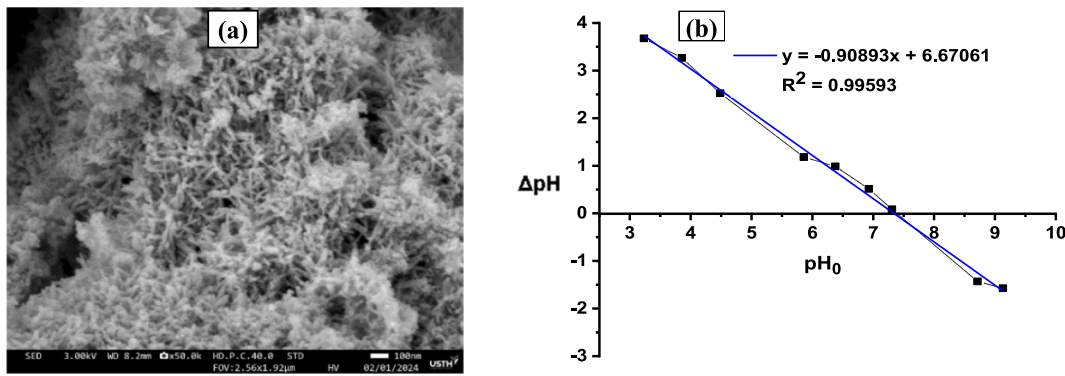


Fig. 1. SEM image (a) and determination of pH_{PZC} (b) of HAp powder.

[(1E,4E)- 2,4-dimethyl-1,5-di(thiophen-2-yl) penta-1,4-dien-3-one] (PTCM) and using to adsorb Zn²⁺. The maximum adsorption capacity for Zn²⁺ of the polymer PTCA and polymer PTCM reached very high 729.4 and 652.7 mg g⁻¹, respectively [19]. E.M. Valdés-Rodríguez et al prepared and functionalized of activated carbons from different biomass and their application in the adsorption of heavy metal ions. The maximum adsorption capacity for Zn²⁺ was obtained 1.59; 0.6; 33.3 mg g⁻¹, respectively by using xanthoceras sorbifolia, pinuca bark and walnut shell biomasses [20]. Agricultural wastes-based biosorbents to effectively remove heavy metals from wastewater were reported by Hina Iqbal Syeda et al. The maximum adsorption capacity of orange peel, banana peel, kiwi, corn cob for Zn²⁺ were calculated 56.18; 9.52; 37.03; 63.93 mg g⁻¹ [21]. Zinc ions removal effectiveness closely depends on the type of proposed adsorbent, so there are many materials investigated to reach the highest as possible recovery rate. One of them that could offer high can be calcium hydroxyapatite (HAp). As it is the main component in human and animal bones (about 65–70 % of the mass) and teeth (about 99 % of the mass) even synthetic HAp offers biocompatibility making it a promising material for environmental applications. It can remove some pollutant substances and ions in the water such as Cu²⁺, Pb²⁺, Zn²⁺, Cd²⁺, Co²⁺, Ni²⁺, Hg²⁺ [8,23–31], Cr(III) [30,32], As (V), Se(VI), NO₃⁻, F⁻, PO₄³⁻, phenol, nitrobenzene, Congo red, etc. [7,15,33–36]. The main mechanisms of adsorption process include both ions adsorption on the surface of HAp and ion exchange. The cations exchange with Ca²⁺ ions and the anions exchange with OH⁻ ions in HAp and so it can be easily applied for the removal of zinc ions from wastewater.

Along with adsorption, desorption and recovery of zinc ions are also extremely important to avoid secondary pollution, to reuse useful metals from waste sources and regenerate adsorbent materials, improving economic efficiency. Several methods have been used to desorb heavy metals from materials such as ion exchange method, solvent method (acid, base, salt, ethyl alcohol, etc.), complexation method, extraction method, heat method, etc. [8,37–41]. After desorption, heavy metals are recovered by methods such as chemical precipitation, electrochemical precipitation, etc. This can lead to more difficulty in recovering metals due to the presence of eluent components. Therefore, there are not so many publications providing methods for metal recovery from eluent solvents.

In 2010, Yuan Feng et al used magnetic HAp with a specific surface area of 142.5 m² g⁻¹ synthesized by precipitation method to adsorb Cd

(II) and Zn(II). The maximum adsorption capacities of 1.964 and 2.151 mmol g⁻¹ were observed for Cd(II) and Zn(II) adsorption, respectively. The desorption process was performed with EDTA, HCl, Ca(NO₃)₂ and NaOH solutions. The results obtained show that the most effective solution for the desorption process was EDTA solution which achieved 66.2 % and 67 % for Cd²⁺ and Zn²⁺ release, respectively [26]. In 2022, E.M. Valdés-Rodríguez et al investigated adsorption of Hg²⁺, Pb²⁺, Zn²⁺ using activated carbons which were fabricated from different biomasses and desorption them to regenerate activated carbon adsorbent by HCl and HNO₃ acids. The result showed that recovery performance was Hg²⁺ > Zn²⁺ > Pb²⁺ and activated carbon were regenerated best in HNO₃ acid solution. In general, eluent solutions were used to desorb metal ions from materials. The desorption mechanism of heavy metals out of loaded material is dissolution in solvent or ion exchange [20]. Rafał Panek et al synthesized pure zeolite (Na-X) and a zeolite-carbon composite (Na-X(C)) from fly ash – a waste from conventional hard coal combustion. These materials were investigated as adsorbents of heavy metal ions Pb²⁺ and Zn²⁺ from an aqueous solution. Desorption of Zn²⁺ and Pb²⁺ ions from the Na-X and Na-X(C) surface in single and mixed systems using 0.1 M HCl or 0.1 M NaOH was studied. The results indicated significantly larger desorption using 0.1 M HCl than 0.1 M NaOH and desorption of higher Pb²⁺ ions than Zn²⁺ ions [42].

Although several papers have mentioned Zn²⁺ adsorption by HAp [23,25,26], the publications spontaneously researching on adsorption, desorption, and metal recovery to recycling are limited. Up to date, there are no works announcing the ability to desorb and recover metals by direct electrolysis of the adsorbed material (M–HAp) in reline ionic liquid (Choline Chloride-Urea mixture). This method has the advantage of not requiring eluent solvent, shortening the metal recovery process, friendly electrolysis environment. Moreover, the adsorbent materials can be regenerated.

To date, there are some publications working on the electrochemical precipitation of Cu²⁺, Zn²⁺, Cd²⁺, Co²⁺, and Ni²⁺ ions in deep eutectic reline solvent (DES) [43–52]. In this article, the ability to adsorb Zn²⁺ ions in water using synthetic hydroxyapatite in the nanostructural form was investigated. The desorption and recovery of metallic Zn were then studied by electrochemical precipitation in reline electrolyte as the way of recovery of that metal ions and its further reuse.

2. Experimental and methodology

2.1. Synthesis HAp powder

HAp powder was synthesized by chemical precipitation method in water medium using initial materials Ca(NO₃)₂·4H₂O (98 %, Merck), (NH₄)₂HPO₄ (99 %, Merck) and NH₃ (25–28 %, Merck) (Eq. (2.1)). 0.3 M (NH₄)₂HPO₄ solution was added to 0.5 M Ca(NO₃)₂ solution at a rate of 1 mL min⁻¹. During the reaction, the pH was kept stable at 10–12 with concentrated NH₃ solution and stirring was maintained at a speed of

Table 1

CV scanning parameters of 0.005 M Zn²⁺ and 0.5 g Zn-HAp in reline.

Parameter	Value	Parameter	Value
WE	Au (S = 0.0201 cm ²)	Potential step	0.005 V
RE	Ag AgCl Cl ⁻	Scanning rate	0.02 V/S
CE	Pt grid	V _{reline}	5 mL
Potential range	-0.2 ÷ -1.6 (V)	—	—

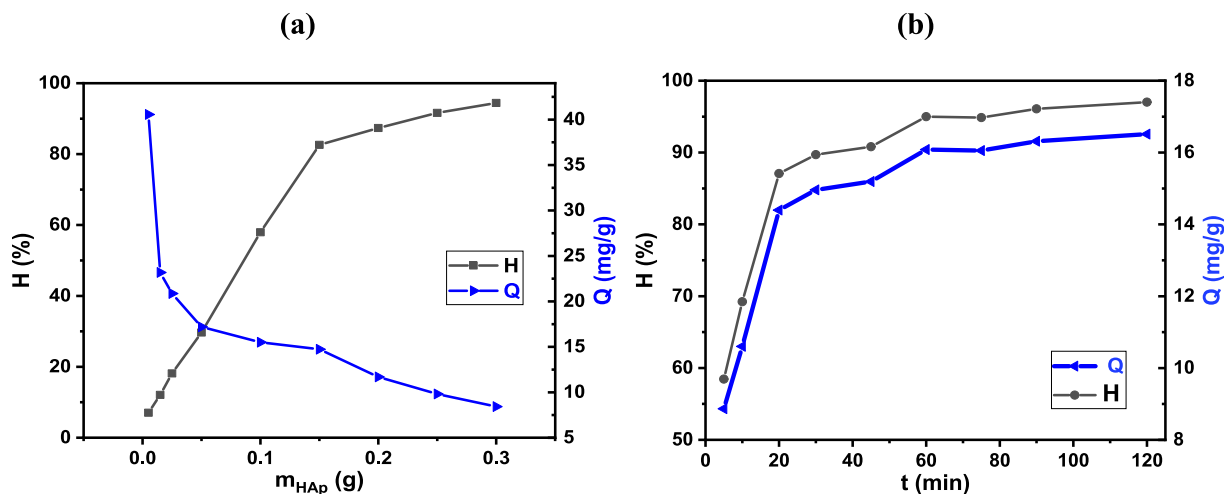


Fig. 2. The effect of HAp mass (at $C_{Zn}^{2+} = 50 \text{ mg.L}^{-1}$, $T = 25^\circ\text{C}$, $\text{pH} = 5.0$, $t = 40 \text{ min}$) (a) and contact time (at $C_{Zn}^{2+} = 50 \text{ mg.L}^{-1}$, $m_{\text{HAp}} = 0.15 \text{ g}$, $T = 25^\circ\text{C}$, $\text{pH} = 5.0$) (b) on the HAp's adsorption of Zn^{2+} .

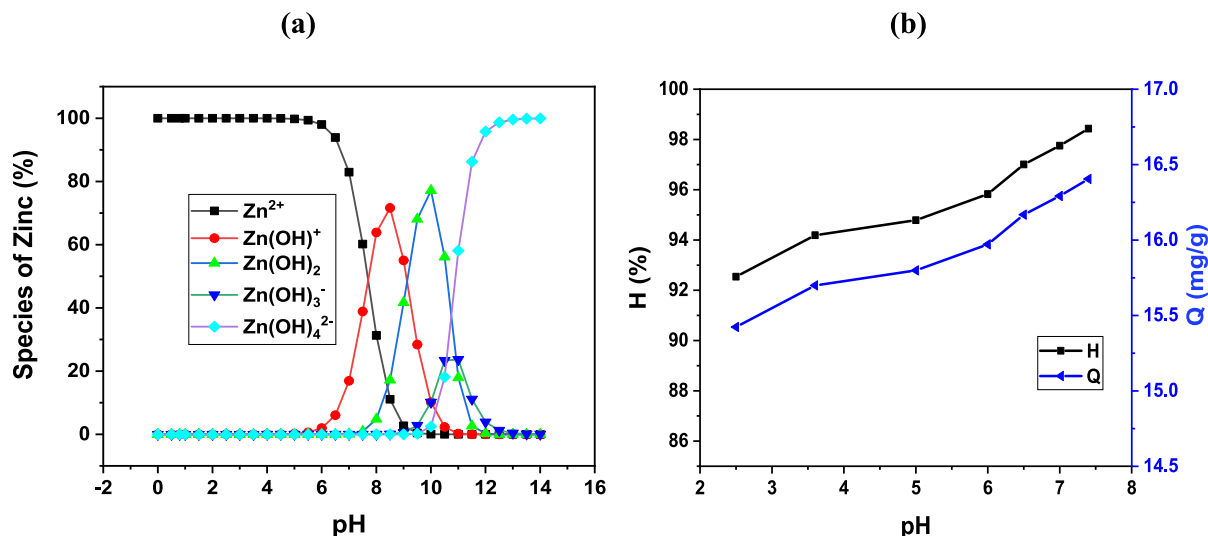
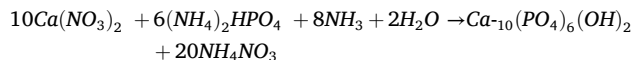


Fig. 3. The variation species of zinc according pH (a) and the effect of pH on the HAp's adsorption of Zn^{2+} (b) at an initial concentration of $50 \text{ mg L}^{-1} \text{ Zn}^{2+}$, HAp dosage of 0.15 g, and contact time of 60 min.

800 rpm. After adding all $(\text{NH}_4)_2\text{HPO}_4$, continued stirring for 2 h. The sample was aged for 15 h, and then washed by centrifuging at 4000 rpm with distilled water until reached neutral pH, dried at 80°C for 24 h and ground in an agate mortar to obtain HAp powder [31].



(2.1)

Synthetic HAp powder studied characterization by methods: FT-IR, SEM, EDX, XRD and BET. The resulting synthetic HAp powder is white, rod-shaped (Fig. 1a) with a specific surface area determined by the Brauner, Emmett and Teller (BET) method of $91.42 \text{ m}^2/\text{g}$.

The pH_{PZC} (Point of Zero Charge) value of the HAp sample was determined using the pH drift method. In this method, 0.1 g of HAp material was added to a 50 mL solution of 0.01 M KCl (purity 99 %, Merck) with varying initial pH values (pH_0), which were adjusted using 0.01 M HCl (purity 37 %, Merck) or 0.01 M NaOH solutions (purity 99 %, Merck). The mixture was then vigorously stirred at 800 revolutions per minute for 30 min using a stirrer. Afterward, the solution was filtered, and the pH (pH_s) of the filtrate was measured to calculate ΔpH

(2.2). A graph was constructed to illustrate the variation of ΔpH with pH_0 . The pH_{PZC} value was identified as the pH_0 at which $\Delta\text{pH} = 0$. The results indicate that $\Delta\text{pH} = 0$ occurs at a pH_0 value of 7.34 (Fig. 1b). This confirms that the pH_{PZC} of the HAp particles is 7.34.

$$\Delta\text{pH} = \text{pH}_0 - \text{pH}_s \quad (2.2)$$

2.2. Adsorption of Zn^{2+} using HAp powder

As the adsorption efficiency depends on many experimental factors, the influence of factors: contact time, pH, adsorbent mass, initial Zn^{2+} solution concentration on the adsorption process was conducted by adding a quantity of HAp powder into a container of 50 mL Zn^{2+} solution with initial concentration in the range of $10\text{--}300 \text{ mg L}^{-1}$, adsorption time varying from 5 – 120 min, pH of the solution 2.5–7.4, HAp powder mass 0.01–0.15 g. The mixture was then stirred at a speed of 400 rpm. After adsorption process, the solution was filtered to separate the solids and the remaining Zn^{2+} ions were quantified using the Inductively Coupled Plasma Mass Spectrometry (ICP-MS) method on ICAP Q ICP-MS (plasma exhaust 0.5–0.6 mbar, penning pressure 6×10^{-7} mbar, pirani pressure 2.0 mbar, cool gas 14 L min^{-1} , plasma power

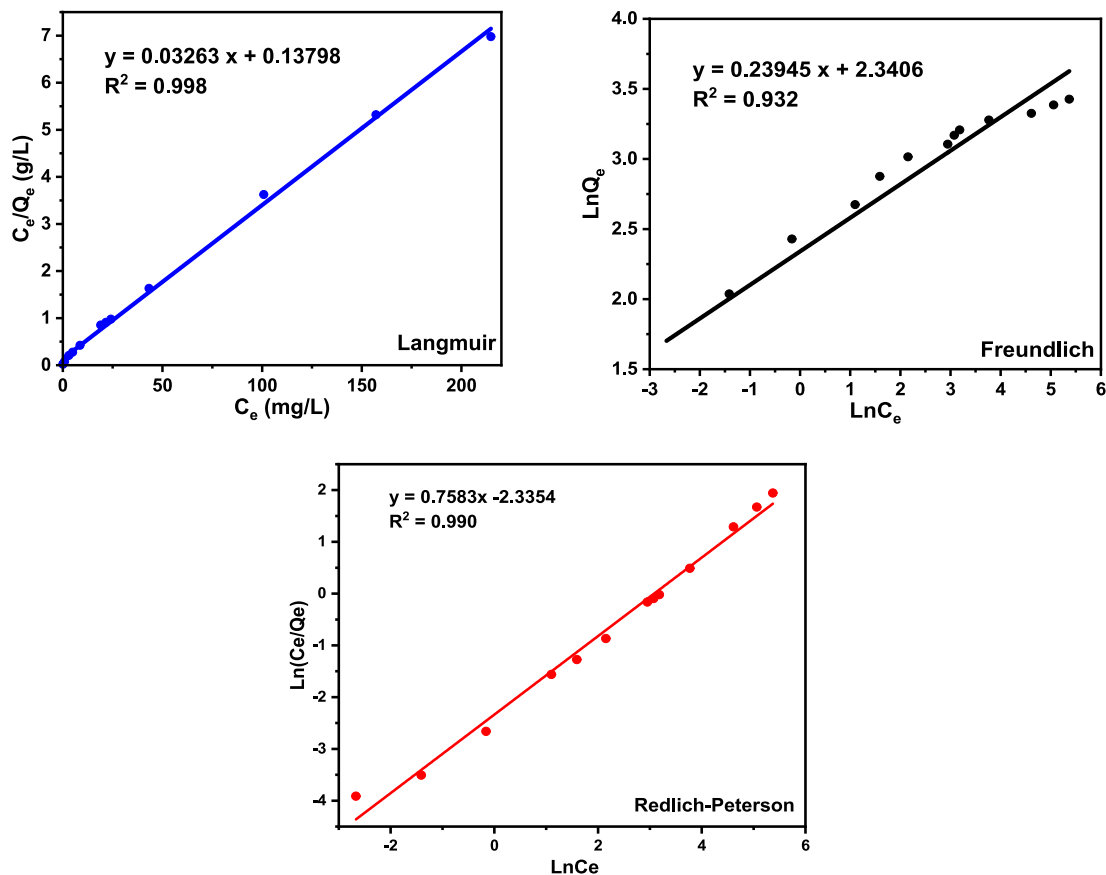


Fig. 4. Adsorption isotherm of Zn²⁺ follow Langmuir, Freundlich and Redlich-Peterson models.

Table 2
Experimental constants Q_m, K_L, K_F, n in the Langmuir and Freundlich equations of Zn²⁺ adsorption process.

Langmuir			Freundlich			Redlich-Peterson		
Q _m	K _L	R ²	n	K _F	R ²	A	B	R ²
30.65	0.2365	0.998	4.1762	10.3875	0.932	0.097	−0.28	0.990

Table 3
The parameters H (%), Q_e (mg.g^{−1}), K_d when changing temperature in the Zn²⁺ adsorption process (mass of HAp = 0.15 g, t = 60 min, pH 5.0).

T (K)	C _e (mg L ^{−1})	H (%)	Q _e (mg g ^{−1})	K _d = Q _e /C _e	lnK _d	1/T
298	3.26	94.72	19.52	5.98	1.79	0.003356
318	1.99	96.78	19.94	10.02	2.30	0.003145
338	0.92	98.51	20.30	22.08	3.09	0.002959
348	0.71	98.86	20.37	28.81	3.36	0.002874

1550 W, uptake time 30 s, wash time 30 s) instrument (Thermo Scientific, Germany).
Adsorption capacity and adsorption efficiency were determined using Eqs. (2.3) and (2.4) [25,29]:

$$Q = (C_0 - C_e) \times V / m \tag{2.3}$$

$$H = \left(\frac{C_0 - C_e}{C_0} \right) \times 100 \tag{2.4}$$

In which: Q (mg g^{−1}) and H (%) are the adsorption capacity and adsorption efficiency, respectively; C₀ (mg L^{−1}) and C_e (mg L^{−1}) are the initial and remaining Zn²⁺ ion concentrations after adsorption, respectively; V is the volume of adsorption solution (L); m is the used mass of HAp powder (g).

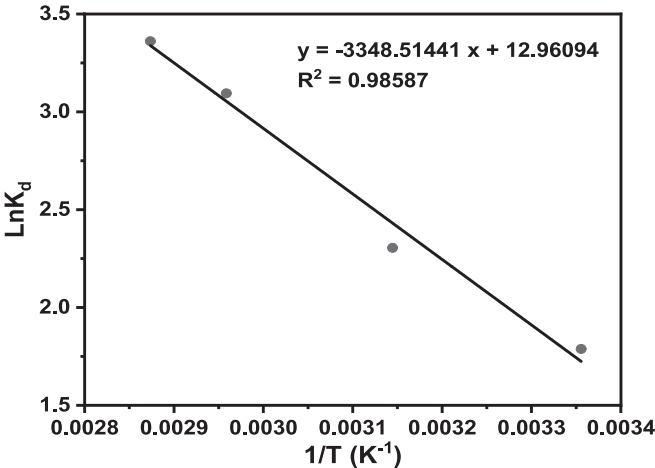


Fig. 5. The variation of LnK_d versus 1/T.

Physicochemical characteristics of HAp before and after Zn²⁺ adsorption was analysed by methods: the phase component was analysed using X-ray diffraction (XRD) (Siemens D5000 diffractometer, CuKα radiation, λ = 1.54056 Å, with a step angle of 0.030°, scanning

Table 4The parameters ΔH° , ΔS° , ΔG° in the Zn^{2+} adsorption process.

T (K)	ΔH° (kJ/mol)	ΔS° (kJ/K)	ΔG° (kJ/mol)
298	27.84	0.108	-4.27
318			-6.50
338			-8.66
348			-9.74

rate of 0.04285°/s, and 2 θ in the range of 10–70°). The structure was analysed by infrared spectroscopy (FT-IR) on a Nicolet iS10 instrument (Thermo Scientific, USA). Morphology and element components were analysed by SEM-EDX on a FE-SEM-JSM-IT800 instrument (JEOL, Japan).

2.2.1. Adsorption isotherm

The Zn^{2+} adsorption ability of HAp was calculated based on the Langmuir, Freundlich [25,29,30] and Redlich-Peterson [53] isotherm models.

$$\text{Langmuir linear equation: } \frac{C_e}{Q} = \frac{C_e}{Q_m} + \frac{1}{K_L \cdot Q_m} \quad (2.5)$$

$$\text{Freundlich linear equation: } \ln Q = \ln K_F + \frac{1}{n} \ln C_e \quad (2.6)$$

$$\text{Redlich – Peterson equation: } \ln \frac{C_e}{Q} = B \ln C_e - \ln A \quad (2.7)$$

where C_e (mg L^{-1}) is the concentration of Zn^{2+} ions at equilibrium, Q (mg g^{-1}) is the adsorption capacity at equilibrium, Q_m (mg g^{-1}) is the maximum adsorption capacity, K_L is the Langmuir coefficient, K_F and n are the Freundlich constants, A is Redlich-Peterson isotherm constant, B is Redlich-Peterson parameter.

2.2.2. Adsorption thermodynamics

Thermodynamic parameters include standard Gibbs free energy change (ΔG°), standard enthalpy change (ΔH°) and standard entropy change (ΔS°) of the Zn^{2+} adsorption process on the synthetic HAp powder was determined using the following equations [25,29,30]:

$$\Delta G^\circ = -RT \ln K_d \quad (2.8)$$

$$\ln K_d = -\frac{\Delta H^\circ}{R} \cdot \frac{1}{T} + \frac{\Delta S^\circ}{R} \quad (2.9)$$

with R is the universal gas constant ($8.314 \text{ J mol}^{-1} \text{ K}^{-1}$), T is the absolute temperature (K), and K_d is the equilibrium constant. The a and b

coefficients (in the linear line $y = ax + b$) of the graph $\ln K_d$ versus $1/T$ are used to determine the values of ΔH° , ΔS° . The value of ΔG° is then calculated according to the expression:

$$\Delta G^\circ = \Delta H^\circ - T\Delta S^\circ \quad (2.10)$$

2.2.3. Adsorption kinetics

The kinetics of the adsorption process was studied according to two kinetic models: pseudo-first-order model (Eq. (2.11)) and pseudo-second-order model (Eq. (2.12)) [25,29,30].

$$\text{The pseudo – first – order model: } \ln(Q_e - Q_t) = \ln Q_e - k_1 t \quad (2.11)$$

$$\text{The pseudo – second – order model: } \frac{t}{Q_t} = \frac{t}{Q_e} - \frac{1}{k_2 Q_e^2} \quad (2.12)$$

In which, Q_e is the adsorption capacity at equilibrium (mg g^{-1}), Q_t is the adsorption capacity at time t (mg g^{-1}), k_1 and k_2 are the first-order rate constant (min^{-1}) and the second-order rate constant ($\text{g mg}^{-1} \text{ min}^{-1}$), respectively.

2.3. Desorption of Zn^{2+} ions and recovery of metallic Zn by electrochemical precipitation

2.3.1. Preparation of reline solvent

Deep eutectic solvent (DES) of reline was made from choline chloride (ChCl , purity $\geq 98\%$, Sigma – Aldrich) and urea (U, 98 %, Sigma – Aldrich). The two solid chemicals were mixed with a molar ratio of 1:2 and stirred at 60 °C for 3 h until a colorless and homogeneous liquid was obtained [54].

2.3.2. Study of the cyclic voltammetry of Zn^{2+} and Zn-HAp in a reline electrolyte

In the cyclic voltammetry (CV) method, a voltage of a specified value is applied to the working electrode and then scanned in the anode or cathode direction to observe the corresponding current. In this measurement method, the electrode surface must be restored before measurement, the solution is not stirred and the mass transfer by diffusion. From the CV curve, it is possible to confirm the electrochemical properties of metal ions under measurement conditions and observe the positions of oxidation and reduction peaks of the metal. On that basis, the necessary voltage to precipitate metal on the cathode electrode is determined.

The CV measuring device includes 3 electrodes immersed in an electrolyte solution: working electrode (WE), reference electrode (RE) and auxiliary electrode/counter electrode (CE) (Table 1).

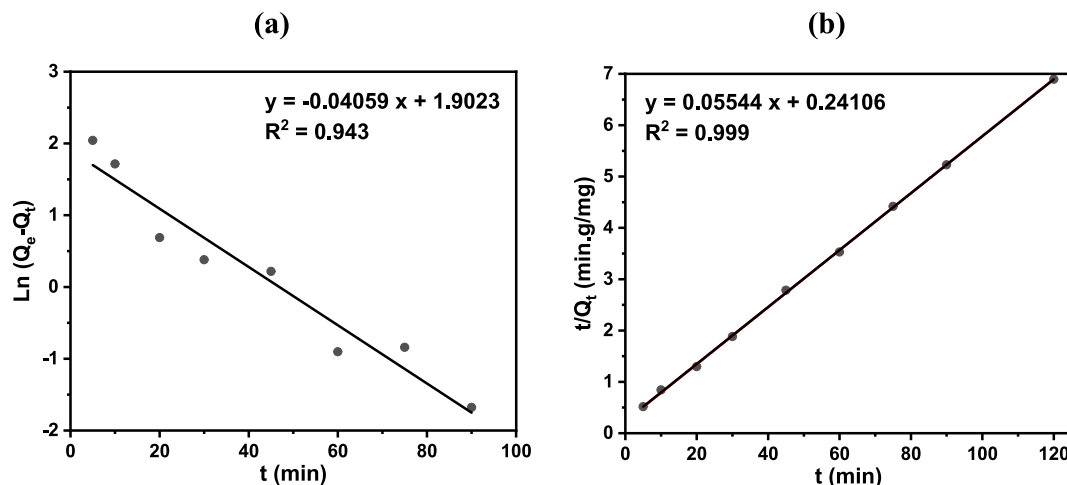


Fig. 6. Kinetic plots for the adsorption of Zn^{2+} onto HAp according to pseudo-first-order kinetic (a) and pseudo-second-order kinetic (b) equations.

Table 5

Values of k and Q_e calculated by pseudo-first-order and pseudo-second-order kinetic equations.

pseudo-first-order kinetic model			pseudo-second-order kinetic model			Q_e exp (mg g^{-1})
Q_e (mg g^{-1})	k_1 (min^{-1})	R^2	Q_e (mg g^{-1})	k_2 ($\text{g mg}^{-1} \text{min}^{-1}$)	R^2	
6.70	0.04059	0.943	18.04	0.01275	0.999	17.40

2.3.3. Desorption of Zn^{2+} and precipitation of metallic Zn on the Au electrode surface

The process of desorption of Zn^{2+} ions from the zinc-adsorbed HAP material (Zn-HAP) and precipitation of Zn metal was carried out in an electrolysis cell using the applied current technique with three electrodes: working electrode was a gold plate (surface geometric area = 1 cm^2 , Germany), reference electrode was an $\text{Ag}|\text{AgCl}|\text{Cl}$ electrode and counter electrode was a platinum mesh with a large area, and it was connected to an Autolab PGSTAT20 potentiostat from Metrohm. Zinc was recovered by electrochemical precipitation in reline solvent at precipitation voltage $\leq -1.06 \text{ V}$, $T = 60^\circ \text{C}$. The DES environment was purged with nitrogen gas for at least 20 min before starting electrolysis and during electrolysis process. Different current values were applied: 1, 2, 3, 5, 7.5 mA; the material mass was varied from 0.1–0.3 g; electrolysis time was studied from 2 to 12 h; temperature of 60°C . After electrolysis, the Zn-HAP powder was filtered out from the mixture, then cleaned, dried, and the amount of remaining Zn in the powder was determined using the ICP-MS method.

3. Results and discussion

3.1. Effect of factors on Zn^{2+} adsorption efficiency and capacity of HAP

3.1.1. Effect of hydroxyapatite mass

The results of the study on the effect of HAP powder mass on the Zn^{2+} adsorption capacity and efficiency are presented in Fig. 2a. As the mass of HAP powder increases from 0.005 to 0.15 g, the adsorption capacity decreases from 40.56 to 14.73 mg g^{-1} , and the adsorption efficiency increases from 7.05 to 82.60 %. When the mass of the adsorbent increases from 0.15 g to 0.3 g, the adsorption efficiency gradually increases and reaches 94.44 % due to the increased contact between the adsorbent and the solution, and the increase in the number of adsorption sites [8,29]. However, the adsorption capacity decreases gradually. To

achieve simultaneous high adsorption capacity and efficiency (14.73 mg g^{-1} ; 82.60 %), a mass of 0.15 g of HAP powder was selected for the study of Zn^{2+} adsorption.

3.1.2. Effect of adsorption time

The variation of the adsorption efficiency and capacity of HAP over time is listed in Fig. 2b. During the observation period, both the adsorption capacity and efficiency increase rapidly in the first 45 min. From 45 min onwards, the adsorption capacity and efficiency increase slowly and stabilize around 16 mg g^{-1} ; 95 % from 60 min onwards due to reaching adsorption equilibrium. To achieve an appropriate magnitude of adsorption capacity and efficiency without prolonging the adsorption time, the appropriate adsorption time is conducted within 60 min and is used for further study.

3.1.3. Effect of pH

The removal of Zn^{2+} ions depends greatly on the pH of the solution because pH alters the surface properties of the adsorbent and the forms of metal ions present in the solution [55]. The forms of zinc ions are indicated on Fig. 3a which is the same according to the publication by R. R. Sheha [25], $\text{Zn}(\text{OH})_2$ begins to precipitate at pH 7.5. From pH_{pzc} 7.34, the experiments were investigated at a range pH of around of 7.34. However, to avoid the precipitation of $\text{Zn}(\text{OH})_2$, the effect of pH was investigated under conditions of $\text{pH} \leq 7.4$. Within this pH range, the main form of zinc in the solution is Zn^{2+} . The results of the variation in adsorption capacity and efficiency of HAP according to pH are presented in Fig. 3b.

From here, it is observed that within the pH range studied, the adsorption efficiency and capacity increase as the pH increases. This result is explained by the fact that in an acidic environment, the surface of HAP particles is protonated, leading to a positively charged surface, which reduces the number of adsorption sites and causes competitive adsorption between H^+ and Zn^{2+} ions [8,29], thereby decreasing the adsorption capacity of HAP at low pH. On the other hand, at low pH, HAP powder is dissolved partly, leading to a decrease in adsorption capacity and efficiency. As pH increases, the positive charge density on the surface decreases, enhancing the ability to adsorb Zn^{2+} ions until reaching a pH higher than pH_{pzc} (7.34), which is favorable for Zn^{2+} ions adsorption, adsorption efficiency and capacity will increase rapidly. At the pH of 5.0 (initial pH), that although smaller than pH_{pzc} but adsorption efficiency and capacity still reach quite high values (94.79 %; 15.80 mg g^{-1}). Therefore, for an efficient treatment process, especially

Table 6

Comparison of the max adsorption capacity and adsorption efficiency of HAP and HAP-based adsorbents for heavy metals relative to our work.

Adsorbents	Adsorbate (heavy metal ions)	pH	Temperature ($^\circ \text{C}$)	Q_m (mg g^{-1})	H %	Ref.
Calcium hydroxyapatite	Zn^{2+}	6–8	30	102.04 mg.g^{-1}	–	[25]
Magnetic hydroxyapatite nanoparticles	Zn^{2+}	5	25	140.63 mg.g^{-1}	–	[26]
Hydroxyapatite	Cd^{2+}	5	25	220.77 mg.g^{-1}	–	[26]
	Zn^{2+}			$0.993 \text{ mmol g}^{-1}$	–	
	Cd^{2+}			$1.137 \text{ mmol g}^{-1}$	–	
Hydroxyapatite	Zn^{2+} 50 mg L^{-1}	5	room temp	57.504 mg g^{-1}	40.36	[27]
Hydroxyapatite	Zn^{2+} 50 mg L^{-1}	5	25	30.65 mg g^{-1}	94.79	This study
Hydroxyapatite/ Fe_3O_4 /polydopamine	Co^{2+} 10 mg L^{-1}	6	25	49.32 mg g^{-1}	90 (the highest)	[28]
	Hg^{2+} 10 mg L^{-1}			51.73 mg g^{-1}	90 (the highest)	
	Ni^{2+} 10 mg L^{-1}			48.09 mg g^{-1}	90 (the highest)	
	Pb^{2+} 10 mg L^{-1}			–	92	
Hydroxyapatite	Co^{2+} 10 mg L^{-1}	5.6	30	–	81.57	[29]
	Ni^{2+} 10 mg L^{-1}			–	6	
	Pb^{2+} 10 mg L^{-1}			12.04 mg g^{-1}	93.5	
	Co^{2+} 10 mg L^{-1}			10.63 mg g^{-1}	88.72	
Hydroxyapatite/chitosan composite	Ni^{2+} 10 mg L^{-1}	6	30	8.54 mg g^{-1}	80	[29]
	Pb^{2+}			7.99 mg g^{-1}	95.92	
	$\text{Cr}(\text{III})$ 100 mg L^{-1}			12.89 mg g^{-1}	–	
	$\text{Cr}(\text{III})$ 100 mg L^{-1}			9.03 mg g^{-1}	–	
Hydroxyapatite granules	Pb^{2+}	5.5	30	7.99 mg g^{-1}	95.92	[31]
Hydroxyapatite/carboxymethyl cellulose composite	$\text{Cr}(\text{III})$ 100 mg L^{-1}	–	20	12.89 mg g^{-1}	–	[32]
Nano hydroxyapatite	$\text{Cr}(\text{III})$ 100 mg L^{-1}			9.03 mg g^{-1}	–	

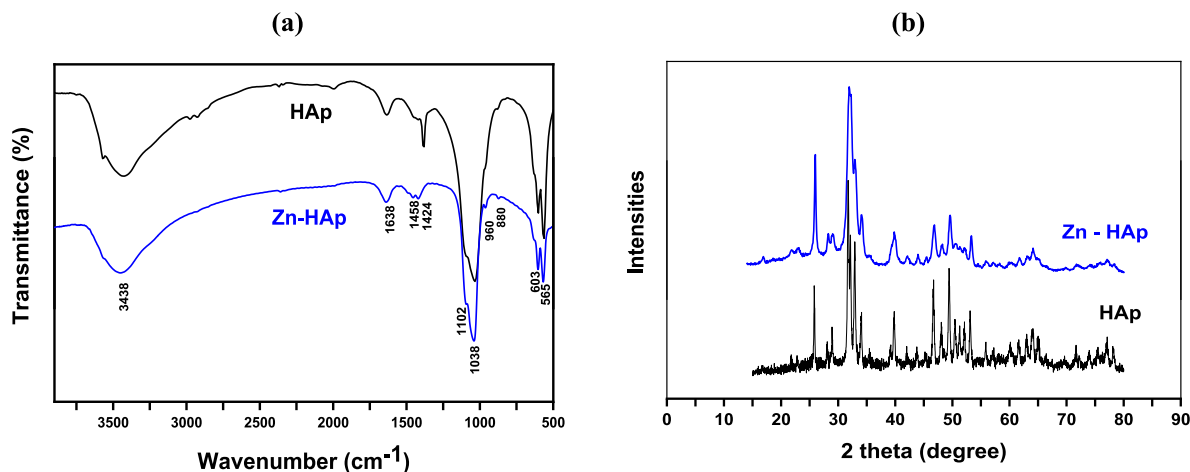


Fig. 7. FT-IR spectra (a) and XRD patterns (b) of HAp before and after Zn^{2+} adsorption process.

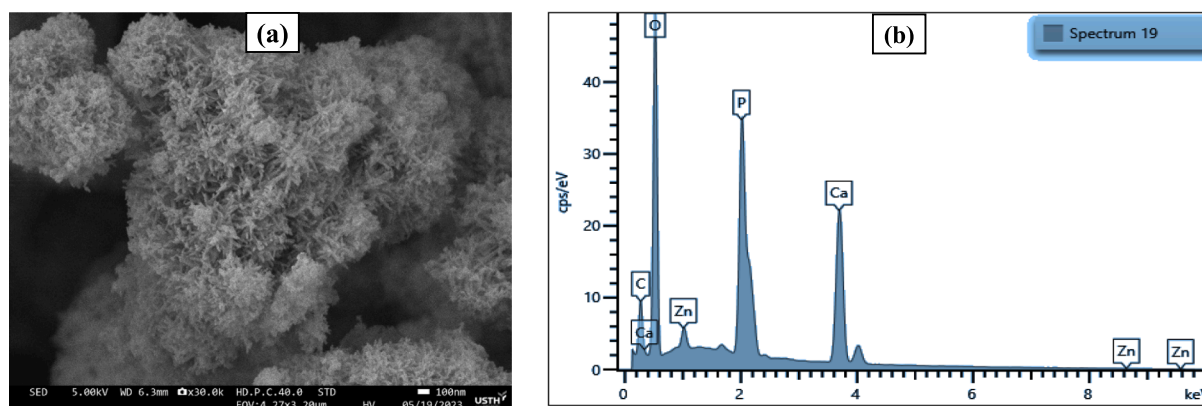


Fig. 8. SEM-EDX analysis of Zn-HAp.

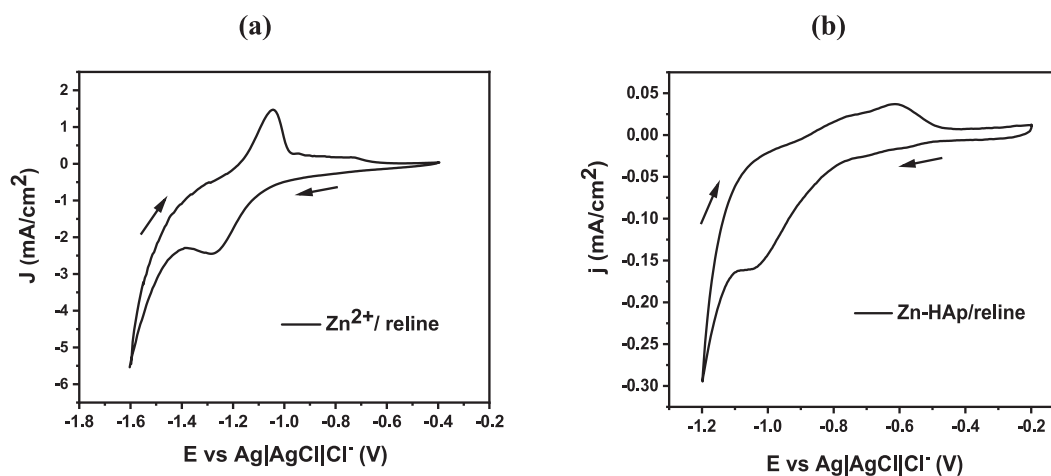


Fig. 9. CV curves of reline containing $\text{Zn}(\text{NO}_3)_2$ (a) and Zn-HAp (b).

in the case of treatment with a large amount of solution, a solution pH of 5.0 (pH_0) is selected for Zn^{2+} adsorption in further studies.

3.2. Adsorption isotherm

The Zn^{2+} adsorption was conducted under the following conditions: 0.15 g of HAp powder, adsorption time of 60 min at a stirring speed of 400 rpm, pH_0 5.0, room temperature (30°C), and 50 mL of Zn^{2+} solution

with varying initial concentrations. Subsequently, the remaining Zn^{2+} concentration at equilibrium (C_e) was determined, from which the values of $\text{Ln}C_e$, $\text{Ln}Q_e$, C_e/Q_e ratio and $\text{Ln}C_e/Q_e$ were calculated, and Langmuir, Freundlich and Redlich-Peterson adsorption isotherm equations were determined (Fig. 4).

The results in Fig. 4 show that the Langmuir model ($R^2 = 0.998$) can be used to describe the experimental data of the Zn^{2+} adsorption process by HAp under the studied conditions better than the Freundlich ($R^2 =$

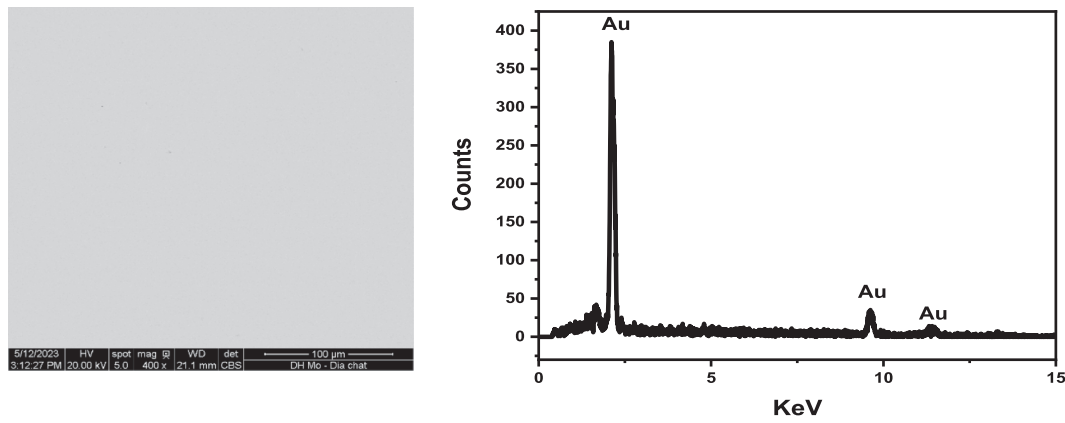


Fig. 10. SEM-EDX analysis of the surface of Au electrode before Zn-HAp electrolysis.

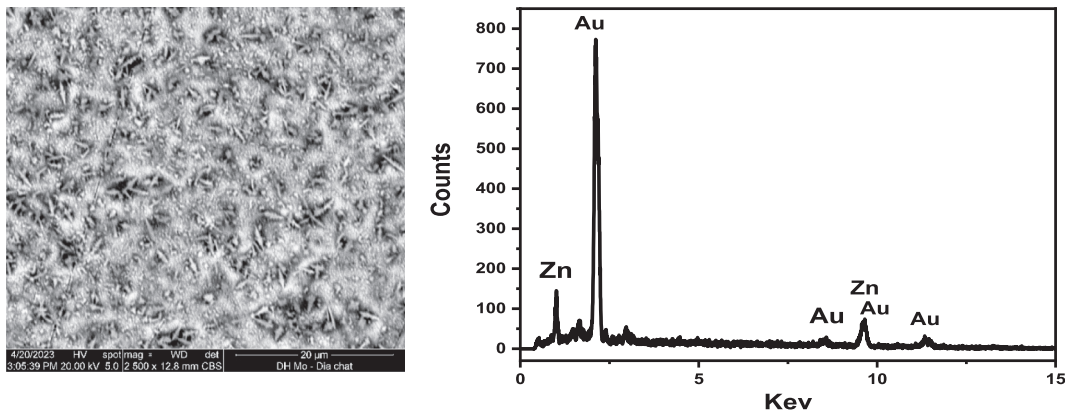


Fig. 11. SEM-EDX analysis of the surface of Au electrode after Zn-HAp electrolysis.

Table 7

Zn recovery efficiency from Zn-HAp at different current intensities $t = 5h$, $m_{Zn-HAp} = 0.3 g$, $T = 60 ^\circ C$.

I (mA)	1.0	2.0	3.0	5.0	7.5
H %	34.23	48.44	56.49	65.81	72.78

Table 8

Zn recovery efficiency from Zn-HAp with different Zn-HAp mass $t = 5h$, $I = 7.5 mA$, $T = 60 ^\circ C$.

m (g)	0.1	0.2	0.3
H %	83.55	79.43	72.78

0.932) and Redlich-Peterson ($R^2 = 0.990$) models. This is consistent with literature on HAp and adsorbents based on HAp for the adsorption of heavy metal ions [8,24–26,29,30]. From the Langmuir isotherm curve, the maximum adsorption capacity of Zn^{2+} (Q_m) can be calculated as $30.65 mg g^{-1}$ (Table 2).

3.3. Adsorption thermodynamic

The adsorption thermodynamic investigation is important to evaluate the spontaneous or unspontaneous adsorption process. The impact of temperature was tested. When increasing the temperature of the adsorption process, the adsorption efficiency and capacity also increase (Table 3). The thermodynamic parameters including standard Gibbs free energy change (ΔG°), standard enthalpy change (ΔH°), and standard entropy change (ΔS°) of the Zn^{2+} adsorption process on HAp powder were determined using equations (2.7) and (2.8). From the calculated

results in Table 3, a graph of $\ln K_d$ against $1/T$ was plotted (Fig. 5), from which the values of ΔG° , ΔH° , and ΔS° were calculated and listed in Table 4. The obtained results express negative values of ΔG° and positive values of ΔH° , indicating that the adsorption process is spontaneous and endothermic.

3.4. Adsorption kinetics

Fig. 6a presents the kinetic data using the Lagergren pseudo-first-order equation, and Fig. 6b shows the kinetic data according to the pseudo-second-order equations of McKay and Ho. The linear relationship with a high correlation coefficient ($R^2 = 0.999$) between t/Q_t and t indicates that the adsorption of Zn^{2+} on HAp is more suitable for the pseudo-second-order model than the pseudo-first-order model ($R^2 = 0.943$). The calculated parameters according to these models are performed in Table 5.

Based on the graphs obtained in Fig. 6, the rate constant (k) and the adsorption capacity at equilibrium (Q_e) were calculated (Table 5). The value of Q_e calculated according to the pseudo-first-order kinetic equation ($6.70 mg g^{-1}$) differs significantly from the experimentally determined Q_e value ($17.40 mg g^{-1}$) which is similar compared to the Q_e value calculated according to the pseudo-second-order kinetic adsorption equation ($18.04 mg g^{-1}$). Furthermore, the regression coefficient of the pseudo-second-order kinetic equation is $R^2 = 0.999 \approx 1$, meanwhile the regression coefficient of the pseudo-first-order kinetic equation (0.943) is far different from 1. This result indicates that the adsorption of Zn^{2+} by HAp follows a pseudo-second-order kinetic adsorption equation. The obtained results are consistent with numerous previous publications [8,24–26,29,30]. The determined rate constant of adsorption process is $0.01275 g mg^{-1} min^{-1}$.

Table 9

Zn recovery efficiency from 0.1 g Zn-HAp at current intensity of 7.5 mA and different electrolysis times.

t (h)	2	3	4	5	6	8	10	12
H %	84.95	87.24	90.68	83.55	86.34	90.72	93.26	95.08

Table 10

Effect of temperature on Zn recovery efficiency $t = 10$ h, $m_{\text{Zn-HAp}} = 0.1$ g, $I = 7.5$ mA.

T (°C)	50	60	70	80
H %	86.73	93.26	94.14	94.76

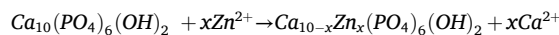
The calculated results exhibit that the maximum adsorption capacity of HAp for Zn^{2+} ions is 30.65 mg g^{-1} , and the adsorption efficiency reaches 94.79 % at a Zn^{2+} concentration of 50 mg L^{-1} . This result shows a higher adsorption efficiency compared to some publications using HAp or HAp's composites for Zn^{2+} and other heavy metal ions adsorption. However, the maximum adsorption capacity is lower than some publications using HAp for Zn^{2+} adsorption and higher than modified HAp for other heavy metal ions adsorption (Table 6). This which can be explained due to our research conducted at lower pH. In addition, we used more mass of HAp powder, so adsorption capacity obtained smaller, but adsorption efficiency was higher than many other publications.

3.5. Characterization of HAp before and after the adsorption process

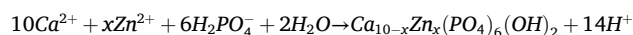
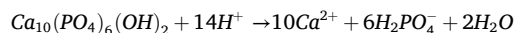
The characteristics of HAp powder before and after the adsorption process were analyzed using FT-IR, XRD, and SEM-EDX. The FT-IR spectra shows that the Zn^{2+} adsorption process does not alter the functional groups in the HAp molecule (Fig. 7a). The absorption bands in the region of 1102; 1038; 960; 603; and 585 cm^{-1} are characteristic of the PO_4^{3-} group. The absorption band of the P-OH bond is located at 880 cm^{-1} . The absorption bands of free water are located at 3438; and 1638 cm^{-1} . The X-ray diffraction patterns of HAp powder samples before (HAp) and after Zn^{2+} adsorption (Zn-HAp) (Fig. 7b) are similar. The two most characteristic diffraction angles of HAp are at positions $2\theta = 31.76^\circ$ and 25.85° . SEM images of HAp after Zn^{2+} adsorption (Fig. 8a) show that the surface morphology of both the original HAp (Fig. 1) and HAp after Zn^{2+} adsorption are rod-like shape. After the Zn^{2+} adsorption process, there is no significant change in the size and shape of the particles. The obtained results are almost identical in terms of the IR and XRD spectra of HAp before and after the adsorption process, which may be explained by the small amount of Zn entering the crystal structure of HAp and replacing Ca, not enough to completely replace all Ca in HAp to form ZnHAp, although many studies have reported on the ion exchange mechanism between Zn^{2+} and Ca^{2+} in HAp [25–27]. The presence of Zn

in HAp after the adsorption process is confirmed by EDX spectrum (Fig. 8b).

Based on the results of characterization of HAp before and after the adsorption process as well as other references, it can be proposed the Zn^{2+} adsorption mechanism as following, where Zn^{2+} ions undergo exchange reaction with the Ca^{2+} ions of HAp as follows:



Futhermore, at low pH the dissolution a part of HAp in aqueous solution containing Zn^{2+} ions then the reaction can occur as follows:

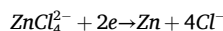


3.6. Desorption of Zn^{2+} and recovery of Zn metal

3.6.1. Cyclic voltammograms of $\text{Zn}(\text{NO}_3)_2$ and Zn-HAp in reline electrolyte

The results indicate the presence of a reduction peak of Zn^{2+} at -1.3 V and an oxidation peak of Zn^0 at -1.05 V on the CV curve of $\text{Zn}(\text{NO}_3)_2$ /reline (Fig. 9a). This observation aligns with previous reports on the CV curve of reline containing Zn^{2+} [45,47,48]. Furthermore, Fig. 9b demonstrates the presence of a reduction peak of Zn^{2+} at -1.06 V and an oxidation peak of Zn^0 at -0.6 V on the CV curve of reline containing Zn-HAp. However, there is a transfer of peaks that observed from $\text{Zn}(\text{NO}_3)_2$ due to the appearance of HAp. The mechanism of the deposition and dissolution of Zn on the Au electrode can be described as following [47,48,50–52]:

Step 1: Formation of a complex between Zn^{2+} from Zn-HAp and Cl^- from reline, resulting in ZnCl_4^{2-} . Subsequently, the reduction of Zn^{2+} (in ZnCl_4^{2-}) to Zn metal occurs on the surface of the electrode:



Step 2: Stripping of Zn metal to Zn^{2+} : $\text{Zn} - 2e \rightarrow \text{Zn}^{2+}$.

The CV results for Zn^{2+} and Zn-HAp in the reline solvent demonstrate that Zn^{2+} ions can be desorbed from the loaded HAp material and subsequently reduced to Zn metal on the surface of an Au electrode in reline solvent, allowing for the recovery and reuse of the HAp adsorbent. The deposition of Zn metal onto the Au electrode surface can be achieved at the potential ≤ -1.06 V.

3.6.2. Effect of several impacts on the ability of Zn^{2+} desorption from HAp and zinc recovery

Zn^{2+} ions were successfully desorbed from Zn-HAp, and Zn metal was efficiently recovered through the electrochemical precipitation method into reline solvent, utilizing applied current technique. The deposition of Zn on the surface of the Au electrode is visually depicted in Figs. 10 and 11.

SEM images show that the surface of the Au electrode before

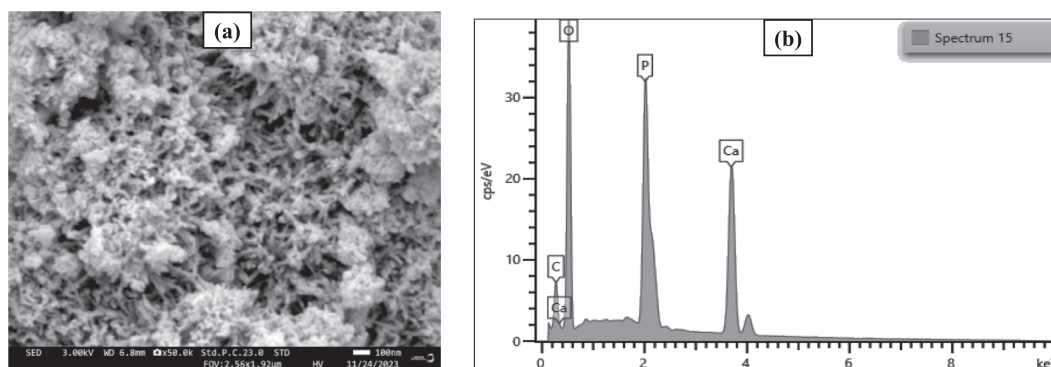


Fig. 12. SEM (a) and EDX (b) analysis of the HAp material after the desorption.

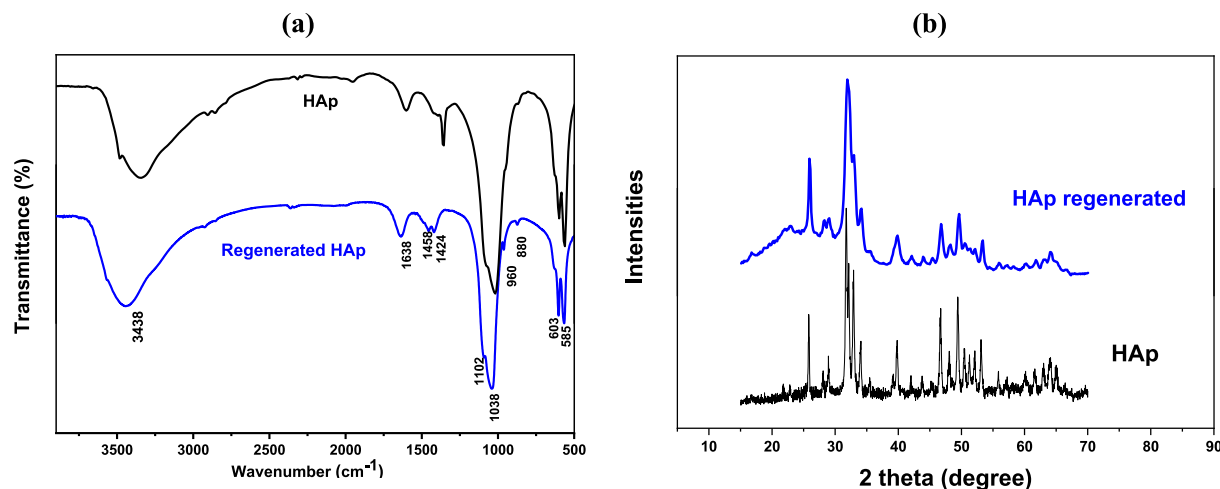


Fig. 13. FT-IR spectra of original HAp, regenerated HAp (a) and XRD pattern of original HAp, regenerated HAp (b).

Table 11

Adsorption capacity and efficiency of Zn^{2+} ions using regenerated HAp material.

Initial Zn^{2+} concentration C_o (mg L^{-1})	Remained Zn^{2+} concentration C_e (mg L^{-1})	Adsorption efficiency H (%)	Adsorption capacity Q (mg g^{-1})
50	6.860	86.28	14.38

electrolysis is smooth (Fig. 10), but there is an even metal layer after electrolysis (Fig. 11). EDX analysis shows that the surface of the Au electrode before electrolysis has no Zn peak, but after Zn-HAp electrolysis, Zn peak appears.

a. Effect of electrolysis current intensity

Polarization of the cathode (Au electrode) at different current intensities was carried out in 5 h at a temperature of 60 °C. The Zn recovery efficiency is provided in Table 7.

The results show that Zn^{2+} was desorbed from Zn-HAp and Zn metal precipitated on the Au electrode surface. Increasing the applied current intensity leads to an increase in the amount of Zn precipitated on the Au electrode surface, thus increasing the Zn^{2+} recovery efficiency (Table 7). Zn recovery efficiency reached 72.78 % after 5 h of electrolysis at a current intensity of 7.5 mA.

b. Effect of mass of Zn-HAp

The variation of Zn recovery efficiency depending on the Zn-HAp mass is shown in Tab. 8. The increasing in Zn-HAp mass leads to an increase in the amount of Zn precipitated on the Au electrode surface but a decrease in Zn recovery efficiency (Table 8). 0.1 g Zn-HAp was chosen for further research to obtain recovery efficiency about 83.55 %.

c. Effect of electrolysis time

Table 9 describes the variation of Zn ions recovery efficiency according to electrolysis time. Increasing electrolysis time leads to an increase in the amount of Zn precipitated on the Au electrode surface, thus increasing the Zn recovery efficiency. To obtain high Zn recovery efficiency (93.26 %) without prolonging the electrolysis time, a time of 10 h was chosen for further research.

d. Effect of electrolysis temperature

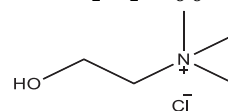
The variation of Zn recovery efficiency according to temperature is indicated in Table 10. Increased temperature leads to increased diffusion of Zn^{2+} ions, leading to an increase in the amount of Zn^{2+} ions moving to the electrode surface and precipitation on the cathode, thus Zn recovery efficiency increases. With the desire to achieve high Zn recovery efficiency (93.26 %), the required temperature for the electrolysis process is 60 °C. If the temperature continues to increase, the efficiency will not increase significantly, so the appropriate temperature is chosen to be 60 °C. Comparing with the desorption efficiency of Zn^{2+} from Zn-HAp of

73.5, 100, 43.7, 10.2, and 8.9 % by using 0.05 M HCl, 0.1 M CuCl_2 , 0.1 M $\text{Ba}(\text{OH})_2$, 0.1 M CaCl_2 and H_2O , respectively (R.R. Seha [25]), and 67, 3.9, 0.6, 15.4 % by using desorption solvents such as EDTA, HCl, NaOH, $\text{Ca}(\text{NO}_3)_2$, respectively (Y. Feng et al [26]), our research obtained much higher desorption and recovery efficiency of Zn in reline solvent.

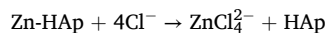
3.7. Mechanism of Zn^{2+} desorption process

Based on the mechanism of electrochemical precipitation of some heavy metals from their salts in reline solvent according to reference documents, and also based on the results of SEM-EDX analysis of the Au plate electrode surface, analysis of Zn-HAp compound after electrolysis showed that Zn^{2+} ions were released during the electrolysis of Zn-HAp and precipitated on the Au electrode surface in the reline electrolyte. Therefore, it can be proposed a mechanism to desorb Zn^{2+} ions from the adsorbed HAp material (M-HAp) and recover M^{n+} ions metal by electrochemical precipitation method as follows:

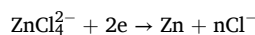
In the formula of choline chloride, a component of the reline solvent, containing Cl^- with molecular formula $\text{C}_5\text{H}_{14}\text{ClNO}$ and structural formula $\text{HOCH}_2\text{CH}_2(\text{CH}_3)_3\text{N}^+\text{Cl}^-$, so the amount of Cl^- in reline is very high:



Step 1: Complexation reaction of Zn^{2+} in Zn-HAp with Cl^- ion in reline:



Step 2: The process of reducing Zn^{2+} in the ZnCl_4^{2-} complex to Zn metal and precipitating on the Au electrode surface:



3.8. Regeneration of material after the desorption

During the electrolysis process, Zn^{2+} ions were successfully desorbed from the loaded HAp material, allowing for the recovery of HAp material for further adsorption.

a. Physicochemical characterization of regenerated HAp material

HAp material after Zn^{2+} desorption process was investigated physicochemical characteristics. The results are demonstrated in Figs. 12 and 13. The SEM image of the obtained HAp after electrolysis closely resembles the original HAp material, retaining its rod shape. Additionally, the EDX spectra indicates characteristic peaks of HAp, with no

discernible Zn peaks (Fig. 12). FT-IR spectra and XRD pattern of the original HAp and regenerated HAp (Fig. 13) show no significant differences. Both original HAp and regenerate HAp have HAp's characteristic peaks and without other phases. This suggests that Zn^{2+} ions were effectively released from Zn-HAp, and the HAp material remained unmodified after the electrolysis of Zn-HAp.

b. Evaluation the adsorption potential of regenerated HAp material

HAp powder obtained after the electrolysis process was cleaned, dried to reuse for further adsorption. To assess the regeneration ability of the HAp adsorbent, adsorption experiments were conducted under appropriate conditions for Zn^{2+} adsorption. The results demonstrated that the adsorption capacity and efficiency could reach 14.38 mg g^{-1} and 86.28 %, respectively, after the first adsorption-desorption cycle (Table 11). These findings show that the regenerated HAp material displays significant adsorption capacity and efficiency for Zn^{2+} ions. The electrolysis process effectively desorbs Zn^{2+} ions from the HAp material and does not affect on HAp's structure and characteristics, therefore the adsorbent can be reused for subsequent adsorption processes.

4. Conclusion

This work demonstrates the efficient way to remove Zn^{2+} ions from water solutions and its subsequent recovery using the nanostructural hydroxyapatite, where the optimal experimental conditions were as follows: an initial Zn^{2+} concentration of 50 mg L^{-1} , HAp mass of 0.15 g, pH 5.0, contact time of 60 min at room temperature (25°C), the adsorption capacity and efficiency reached 15.80 mg g^{-1} and 94.79 %, respectively. The adsorption process occurs as endothermic and follows the Langmuir isotherm model with a maximum adsorption capacity of 30.65 mg g^{-1} and pseudo-second-order kinetic model. Importantly, the desorption of Zn^{2+} from the loaded HAp material and the recovery of Zn metal were conducted simultaneously in a non-toxic reline DES by the electrochemical precipitation method. The results demonstrated that 93.26 % of the Zn metal amount can be recovered under suitable parameters. Following the Zn metal released from the loaded HAp material and HAp can be reused for subsequent adsorption processes. The adsorption capacity and efficiency achieved 14.38 mg g^{-1} and 86.28 %, respectively for reused HAp material under the studied suitable conditions. This outcome opens the potential for utilizing HAp to remove Zn^{2+} ions from polluted water and recover Zn metal directly from loaded material without elute solvent, avoid secondary pollution, and recover useful metals from waste sources.

CRediT authorship contribution statement

Le Thi Duyen: Conceptualization, Formal analysis, Investigation, Methodology, Project administration, Writing – review & editing. **Cong Tien Dung:** Investigation, Writing – original draft. **Dinh Thi Mai Thanh:** Supervision. **Nguyen Thu Phuong:** Investigation, Writing – original draft.

Declaration of competing interest

The authors declare that they have no known competing financial interests or personal relationships that could have appeared to influence the work reported in this paper.

Data availability

No data was used for the research described in the article.

Acknowledgments

The authors thank the project of the Ministry of Education and Training of Vietnam, the code number B2022-MDA-03 for helping complete this research.

References

- [1] B. Bai, F. Bai, X. Li, Q. Nie, X. Jia, H. Wu, The remediation efficiency of heavy metal pollutants in water by industrial red mud particle waste, *Environ. Technol. Innov.* 28 (2022) 102944, <https://doi.org/10.1016/j.eti.2022.102944>.
- [2] E. Kuldeyev, M. Seitzhanova, S. Tanirbergenova, K. Tazhu, E. Doszhanov, Z. Mansurov, S. Azat, R. Nurlybaev, R. Berndtsson, Modifying natural zeolites to improve heavy metal adsorption, *Water* 15 (2023), <https://doi.org/10.3390/w15122215>.
- [3] T. Do, P. Tran, M.-V. AnhKhoaTon, A novel method for the fabrication of granular hydroxyapatite-bentonite composite adsorbents for the removal of Pb^{2+} from an aqueous solution, *J. Environ. Sci. Eng. B* 5 (2016), <https://doi.org/10.17265/2162-5263/2016.07.008>.
- [4] M. Quaghebeur, A. Rate, Z. Rengel, C. Hinz, Heavy metals in the environment desorption kinetics of arsenate from kaolinite as influenced by pH, *J. Environ. Qual.* 34 (2005) 479–486, <https://doi.org/10.2134/jeq2005.0479a>.
- [5] M. Aliabadi, M. Irani, J. Ismaeili, S. Najafzadeh, Design and evaluation of chitosan/hydroxyapatite composite nanofiber membrane for the removal of heavy metal ions from aqueous solution, *J. Taiwan Inst. Chem. Eng.* 45 (2014) 518–526, <https://doi.org/10.1016/j.jtice.2013.04.016>.
- [6] M.S. Fernando, R.M. de Silva, K.M.N. de Silva, Synthesis, characterization, and application of nano hydroxyapatite and nanocomposite of hydroxyapatite with granular activated carbon for the removal of Pb^{2+} from aqueous solutions, *Appl. Surf. Sci.* 351 (2015) 95–103, <https://doi.org/10.1016/j.apsusc.2015.05.092>.
- [7] A. Bahdod, S. El Asri, A. Saoiabi, T. Coradin, A. Laghzizil, Adsorption of phenol from an aqueous solution by selected apatite adsorbents: Kinetic process and impact of the surface properties, *Water Res.* 43 (2009) 313–318, <https://doi.org/10.1016/j.watres.2008.10.023>.
- [8] P. Chand, Y.B. Pakade, Synthesis and characterization of hydroxyapatite nanoparticles impregnated on apple pomace to enhanced adsorption of Pb(II) , Cd(II) , and Ni(II) ions from aqueous solution, *Environ. Sci. Pollut. Res.* 22 (2015) 10919–10929, <https://doi.org/10.1007/s11356-015-4276-2>.
- [9] I. Anastopoulos, A. Mittal, M. Usman, J. Mittal, G. Yu, A. Núñez-Delgado, M. Kornaros, A review on halloysite-based adsorbents to remove pollutants in water and wastewater, *J. Mol. Liq.* 269 (2018) 855–868, <https://doi.org/10.1016/j.molliq.2018.08.104>.
- [10] P. Maziarz, J. Matusik, A. Radziszewska, Halloysite-zero-valent iron nanocomposites for removal of Pb(II) / Cd(II) and As(V) / Cr(VI) : Competitive effects, regeneration possibilities and mechanisms, *J. Environ. Chem. Eng.* 7 (2019) 103507, <https://doi.org/10.1016/j.jece.2019.103507>.
- [11] N.S. Aljohani, Y.N. Kavil, R.K. Al-Farawati, S. Saad Alelyani, M.I. Orif, Y.A. Shaban, S.R. Al-Mhyawi, E.H. Aljuhani, M. Abdel Salam, The effective adsorption of arsenic from polluted water using modified Halloysite nanoclay, *Arab. J. Chem.* 16 (2023) 104652, <https://doi.org/10.1016/j.arabjc.2023.104652>.
- [12] M. Rajiv Gandhi, G.N. Kousalya, S. Meenakshi, Removal of copper(II) using chitin/chitosan nano-hydroxyapatite composite, *Int. J. Biol. Macromol.* 48 (2011) 119–124, <https://doi.org/10.1016/j.jbiomac.2010.10.009>.
- [13] F. Marrakchi, M.J. Ahmed, W.A. Khanday, M. Asif, B.H. Hameed, Mesoporous-activated carbon prepared from chitosan flakes via single-step sodium hydroxide activation for the adsorption of methylene blue, *Int. J. Biol. Macromol.* 98 (2017) 233–239, <https://doi.org/10.1016/j.jbiomac.2017.01.119>.
- [14] M.A. Islam, M.J. Ahmed, W.A. Khanday, M. Asif, B.H. Hameed, Mesoporous activated carbon prepared from NaOH activation of rattan (*Lacosperma secundiflorum*) hydrochar for methylene blue removal, *Ecotoxicol. Environ. Saf.* 138 (2017) 279–285, <https://doi.org/10.1016/j.ecoenv.2017.01.010>.
- [15] S. Hokkanen, E. Repo, L.J. Westholm, S. Lou, T. Sainio, M. Sillanpää, Adsorption of Ni^{2+} , Cd^{2+} , PO_4^{3-} and NO_3^- from aqueous solutions by nanostructured microfibrillated cellulose modified with carbonated hydroxyapatite, *Chem. Eng. J.* 252 (2014) 64–74, <https://doi.org/10.1016/j.cej.2014.04.101>.
- [16] M. Hamzaoui, B. Benaouda, N. Benderdouche, The use of linear and nonlinear methods for adsorption isotherm optimization of basic green 4-dye onto sawdust-based activated carbon, *J. Mater. Environ. Sci.* 9 (2018), <https://doi.org/10.26872/jmes.2018.9.4.122>.
- [17] M. Arbabi, S. Hemati, Z. Shamsizadeh, A. Arbabi, Nitrate removal from aqueous solution by almond shells activated with magnetic nanoparticles, *Desalination Water Treat.* 80 (2017) 344–351, <https://doi.org/10.5004/dwt.2017.20999>.
- [18] A.A. Asiri, Selected MRI and organic fluorescence sensors for the recognition of Zn^{2+} ions in biological matrices: A review, *Dyes Pigm.* 219 (2023) 111580, <https://doi.org/10.1016/j.dyepig.2023.111580>.
- [19] P. Sowmya, S. Prakash, A. Joseph, Adsorption of heavy metal ions by thiophene containing mesoporous polymers: An experimental and theoretical study, *J. Solid State Chem.* 320 (2023) 123836, <https://doi.org/10.1016/j.jssc.2023.123836>.
- [20] E.M. Valdés-Rodríguez, D.I. Mendoza-Castillo, H.E. Reynel-Avila, I.A. Aguayo-Villarreal, A. Bonilla-Petriciolet, Activated carbon manufacturing via alternative Mexican lignocellulosic biomass and their application in water treatment: Preparation conditions, surface chemistry analysis and heavy metal adsorption properties, *Chem. Eng. Res. Des.* 187 (2022) 9–26, <https://doi.org/10.1016/j.cherd.2022.08.039>.
- [21] H.I. Syeda, I. Sultan, K.S. Razavi, P.-S. Yap, Biosorption of heavy metals from aqueous solution by various chemically modified agricultural wastes: A review, *J. Water Process Eng.* 46 (2022) 102446, <https://doi.org/10.1016/j.jwpe.2021.102446>.
- [22] K.M. Nguyen, B.Q. Nguyen, H.T. Nguyen, H.T.H. Nguyen, Adsorption of arsenic and heavy metals from solutions by unmodified iron-ore sludge, *Appl. Sci.* 9 (2019), <https://doi.org/10.3390/app9040619>.

- [23] K. Viipsi, S. Sjöberg, K. Tönsuaadu, A. Shchukarev, Hydroxy- and fluorapatite as sorbents in Cd(II)–Zn(II) multi-component solutions in the absence/presence of EDTA, *J. Hazard. Mater.* 252–253 (2013) 91–98, <https://doi.org/10.1016/j.jhazmat.2013.02.034>.
- [24] I. Mobasherpour, E. Salahi, M. Pazouki, Comparative of the removal of Pb^{2+} , Cd^{2+} and Ni^{2+} by nano crystallite hydroxyapatite from aqueous solutions: Adsorption isotherm study, *Arab. J. Chem.* 5 (2012) 439–446, <https://doi.org/10.1016/j.arabjc.2010.12.022>.
- [25] R.R. Sheha, Sorption behavior of Zn(II) ions on synthesized hydroxyapatites, *J. Colloid Interface Sci.* 310 (2007) 18–26, <https://doi.org/10.1016/j.jcis.2007.01.047>.
- [26] Y. Feng, J.-L. Gong, G.-M. Zeng, Q.-Y. Niu, H.-Y. Zhang, C.-G. Niu, J.-H. Deng, M. Yan, Adsorption of Cd (II) and Zn (II) from aqueous solutions using magnetic hydroxyapatite nanoparticles as adsorbents, *Chem. Eng. J.* 162 (2010) 487–494, <https://doi.org/10.1016/j.cej.2010.05.049>.
- [27] S.L. Iconaru, M. Motelica-Heino, R. Guegan, M.V. Predoi, A.M. Prodan, D. Predoi, Removal of zinc ions using hydroxyapatite and study of ultrasound behavior of aqueous media, *Materials (Basel)* 11 (2018), <https://doi.org/10.3390/ma11081350>.
- [28] R. Foroutan, S.J. Peighambaroud, A. Ahmadi, A. Akbari, S. Farjadfar, B. Ramavandi, Adsorption mercury, cobalt, and nickel with a reclaimable and magnetic composite of hydroxyapatite/ Fe_3O_4 /polydopamine, *J. Environ. Chem. Eng.* 9 (2021) 105709, <https://doi.org/10.1016/j.jece.2021.105709>.
- [29] N. Gupta, A.K. Kushwaha, M.C. Chattopadhyaya, Adsorptive removal of Pb^{2+} , Co^{2+} and Ni^{2+} by hydroxyapatite/chitosan composite from aqueous solution, *J. Taiwan Inst. Chem. Eng.* 43 (2012) 125–131, <https://doi.org/10.1016/j.jtice.2011.07.009>.
- [30] Y. Si, J. Huo, Y. Hengbo, A. Wang, Adsorption kinetics, isotherms, and thermodynamics of Cr(III), Pb(II), and Cu(II) on porous hydroxyapatite nanoparticles, *J. Nanosci. Nanotechnol.* 18 (2018) 3484–3491, <https://doi.org/10.1166/jnn.2018.14631>.
- [31] D.T. Le, T.P.T. Le, H.T. Do, H.T. Vo, N.T. Pham, T.T. Nguyen, H.T. Cao, P. T. Nguyen, T.M.T. Dinh, H.V. Le, D.L. Tran, Fabrication of porous hydroxyapatite granules as an effective adsorbent for the removal of aqueous Pb(II) ions, *J. Chem.* 2019 (2019) 8620181, <https://doi.org/10.1155/2019/8620181>.
- [32] Z. Abbasi, E. Ramezani, A. Farrokhnia, A.A. Naseri, A. Sayadi, Hydroxyapatite/carboxymethyl cellulose composite: Synthesis, characterization, kinetic, thermodynamic study for removal of Cr (III), *ALKHAS* 3 (2021) 12–17, <https://doi.org/10.47176/alkhas.3.1.12>.
- [33] M. Islam, P.C. Mishra, R. Patel, Physicochemical characterization of hydroxyapatite and its application towards removal of nitrate from water, *J. Environ. Manage.* 91 (2010) 1883–1891, <https://doi.org/10.1016/j.jenvman.2010.04.013>.
- [34] W. Wei, R. Sun, J. Cui, W. Zhenggui, Removal of nitrobenzene from aqueous solution by adsorption on nanocrystalline hydroxyapatite, *Desalination* 263 (2010) 89–96, <https://doi.org/10.1016/j.desal.2010.06.043>.
- [35] H. Hou, R. Zhou, P. Wu, L. Wu, Removal of Congo red dye from aqueous solution with hydroxyapatite/chitosan composite, *Chem. Eng. J.* 211–212 (2012) 336–342, <https://doi.org/10.1016/j.cej.2012.09.100>.
- [36] S. Pai, S.M. Kini, R. Selvaraj, A. Pugazhendhi, A review on the synthesis of hydroxyapatite, its composites and adsorptive removal of pollutants from wastewater, *J. Water Process Eng.* 38 (2020) 101574, <https://doi.org/10.1016/j.jwpe.2020.101574>.
- [37] H. Tran, N. Vu, M. Matsukawa, M. Okajima, T. Kaneko, K. Ohki, Y. Shinya, Heavy metal biosorption from aqueous solutions by algae inhabiting rice paddies in Vietnam, *J. Environ. Chem. Eng.* 4 (2016), <https://doi.org/10.1016/j.jece.2016.04.038>.
- [38] D.T. Nguyen, D.P. Truong, P. Ning, Sorption of Pb(ii), Cu(ii) and Cd(ii) by biomass of the different activated sludge, *CTU J. Innov. Sustain. Dev.* (2016) 20–27, <https://doi.org/10.22144/ctu.jen.2016.039>.
- [39] V.X. Minh, K.T.T. Dung, P.T. Lan, L.T.M. Hanh, N.T. Dung, Study on Ni(II) adsorption by calcium alginate beads, *Vietnam J. Chem.* 58 (2020) 358–363, <https://doi.org/10.1002/vjch.2019000195>.
- [40] V.T. Le, T.K.N. Tran, D.L. Tran, H.S. Le, V.D. Doan, Q.D. Bui, H.T. Nguyen, One-pot synthesis of a novel magnetic activated carbon/clay composite for removal of heavy metals from aqueous solution, *J. Dispersion Sci. Technol.* 40 (2019) 1761–1776, <https://doi.org/10.1080/01932691.2018.1541414>.
- [41] T.T.N. Le, V.T. Le, M.U. Dao, Q.V. Nguyen, T.T. Vu, M.H. Nguyen, D.L. Tran, H. S. Le, Preparation of magnetic graphene oxide/chitosan composite beads for effective removal of heavy metals and dyes from aqueous solutions, *Chem. Eng. Commun.* 206 (2019) 1337–1352, <https://doi.org/10.1080/00986445.2018.1558215>.
- [42] R. Panek, M. Medykowska, M. Wiśniewska, K. Szweczek-Karpisz, K. Jedruchiewicz, M. Franus, Simultaneous removal of Pb^{2+} and Zn^{2+} heavy metals using fly ash Na-X zeolite and its carbon Na-X(C) composite, *Materials* 14 (11) (2021) 2832, <https://doi.org/10.3390/ma14112832>.
- [43] A. Abbott, A. Ballantyne, R. Harris, J. Juma, K. Ryder, A comparative study of nickel electrodeposition using deep eutectic solvents and aqueous solutions, *Electrochim. Acta* 176 (2015) 718–726, <https://doi.org/10.1016/j.electacta.2015.07.051>.
- [44] P. Sebastián, E. Gómez, V. Climent, J.M. Feliu, Copper underpotential deposition at gold surfaces in contact with a deep eutectic solvent: New insights, *Electrochim. Commun.* 78 (2017) 51–55, <https://doi.org/10.1016/j.elecom.2017.03.020>.
- [45] M. Starykevich, A.N. Salak, D.K. Ivanou, A.D. Lisenkov, M.L. Zheludkevich, M.G. S. Ferreira, Electrochemical deposition of zinc from deep eutectic solvent on barrier alumina layers, *Electrochim. Acta* 170 (2015) 284–291, <https://doi.org/10.1016/j.electacta.2015.04.150>.
- [46] A. Shishov, A. Bulatov, M. Locatelli, S. Carradori, V. Andrich, Application of deep eutectic solvents in analytical chemistry. A review, *Microchem. J.* 135 (2017) 33–38, <https://doi.org/10.1016/j.microc.2017.07.015>.
- [47] S. Spathariotis, Recovery of Metals using Deep Eutectic Solvents, University of Leicester, 2020.
- [48] E. Emanuele, A. Li Bassi, A. Macrelli, C. Mele, J. Strada, B. Bozzini, Zinc electrode cycling in deep eutectic solvent electrolytes: An electrochemical study, *Molecules* 28 (2023), <https://doi.org/10.3390/molecules28030957>.
- [49] J.G. Costa, J.M. Costa, A.F. Almeida Neto, Progress on electrodeposition of metals and alloys using ionic liquids as electrolytes, *Metals* 12 (2022), <https://doi.org/10.3390/met12122095>.
- [50] L. Vieira, A. Whitehead, B. Gollas, Mechanistic studies of zinc electrodeposition from deep eutectic electrolytes, *ECS Trans.* 50 (2013) 83, <https://doi.org/10.1149/05052.0083ecst>.
- [51] N.M. Pereira, C.M. Pereira, J.P. Araújo, A. Fernando Silva, Zinc Electrodeposition from deep eutectic solvent containing organic additives, *J. Electroanal. Chem.* 801 (2017) 545–551, <https://doi.org/10.1016/j.jelechem.2017.08.019>.
- [52] A.H. Whitehead, M. Pölzler, B. Gollas, Zinc electrodeposition from a deep eutectic system containing choline chloride and ethylene glycol, *J. Electrochem. Soc.* 157 (2010) D328, <https://doi.org/10.1149/1.3364930>.
- [53] H.N. Tran, E.C. Lima, R.S. Juang, J.C. Bollinger, H.P. Chao, Thermodynamic parameters of liquid-phase adsorption process calculated from different equilibrium constants related to adsorption isotherms: A comparison study, *J. Environ. Chem. Eng.* 9 (2021) 106674, <https://doi.org/10.1016/j.jece.2021.106674>.
- [54] Q. Rayée, T. Doneux, C. Buess-Herman, Underpotential deposition of silver on gold from deep eutectic electrolytes, *Electrochim. Acta* 237 (2017) 127–132, <https://doi.org/10.1016/j.electacta.2017.03.182>.
- [55] M.A. Abdel-Fadeel, N.S. Aljohani, S.R. Al-Mhyawi, R.F. Halawani, E.H. Aljuhani, M.A. Salam, A simple method for removal of toxic dyes such as Brilliant Green and Acid Red from the aquatic environment using Halloysite nanoclay, *J. Saudi Chem. Soc.* 26 (2022) 101475, <https://doi.org/10.1016/j.jscs.2022.101475>.